ELSEVIER

Comput. Methods Appl. Mech. Engrg. 125 (1995) 235–255

Computer methods in applied mechanics and engineering

Numerical method for coupled fluid flow, heat transfer and stress analysis using unstructured moving meshes with cells of arbitrary topology

I. Demirdžić*, S. Muzaferija

Mašinski fakultet, Omladinsko šetalište bb, Sarajevo, Bosnia and Herzegowina

Received 27 July 1994

Abstract

A numerical method is presented that can be used for both solid body stress analysis and fluid flow predictions, independently as well as in a coupled manner. The method uses an integral form of equations governing mass, energy and momentum balance for an arbitrary control volume. A detailed description is provided of a novel second-order accurate spatial discretisation technique which can accommodate unstructured moving meshes with cells of arbitrary topology. This is accompanied by a fully implicit temporal discretisation, which makes the method stable for any time step size. The resulting set of coupled non-linear algebraic equations is solved by employing a segregated approach, leading to a decoupled set of linear algebraic equations for each dependent variable, with a sparse diagonally dominant coefficient matrix. These equations are solved by an iterative conjugate gradient solver which retains the sparsity of the coefficient matrix, thus achieving a very efficient use of computer resources.

The method has been tested on a number of fluid flow and stress analysis problems and numerical calculations show favourable agreement with analytical and/or experimental results. In order to demonstrate the full capabilities of the present method, an example of numerically complex coupled fluid flow, stress analysis and heat transfer calculations is presented.

1. Introduction

Continuum mechanics is conventionally subdivided into solid mechanics and fluid mechanics and, traditionally, problems involving an interaction between fluid flow and heat transfer and resulting deformations and stresses in the solid structure in contact with the flow (heat exchangers, wind loaded structures, internal combustion engines, etc.) are treated separately, in a decoupled manner, often using completely different (analytical or numerical) solution techniques. There is, however, a wide range of problems that require a simultaneous solution of fluid flow and solid body deformation, to mention only a few: casting of metal components, which involves a continuous transformation from flowing liquid to a deforming solid as one of the key features of the process, welding, where a region of flowing liquid 'travels through' the deforming solid [1], or interaction of vortex shading and fluid flow-induced oscillations of solid structures [2].

The fact that solid body and fluid mechanics share the same governing equations and differ in constitutive relations only is used in this paper to develop a numerical method for a simultaneous (coupled) solution of the above problems. The method is based on the solution of an integral form of conservation equations governing mass, energy and momentum balance on a numerical mesh consisting

* Corresponding author at: Computational Dynamics Ltd., Olympic House, 317 Latimer Road, London W10 6RA, UK.

SSDI 0045-7825(95)00800-4

of a finite number of contiguous control volumes of completely arbitrary topology. A newly developed procedure is employed to approximate spatial distribution of dependent variables (which can accommodate arbitrary topology of the mesh). A collocated variable arrangement is used, i.e. all dependent variables are stored at the geometrical centres of control volumes, and a segregated approach is employed to solve resulting set of coupled non-linear algebraic equations, embedding a SIMPLE based algorithm for calculation of pressure in fluids.

2. Mathematical formulation

In this section the mathematical model of deformation of solids, flow of fluids and conjugate heat transfer is presented. It includes the mass, momentum and energy balance equations in an integral form, a space conservation equation, which has to be satisfied if the problem is solved on a moving mesh, constitutive relations required for the problem closure and boundary conditions usually encountered in practical applications. Although the method is applicable to any type of solid and fluid material, the constitutive relations for thermo-elastic solid and Newtonian fluid are used for illustrative purposes.

2.1. Governing equations

The behaviour of continuum (both solid and fluid) is governed by the following transport equations:

- mass balance or continuity equation

$$\frac{\partial}{\partial t}\int_V \rho \, \mathrm{d}V + \int_S \rho(\boldsymbol{v} - \boldsymbol{v}_s)\cdot \mathrm{d}\boldsymbol{s} = 0 , \tag{1}$$

- equation of thermal energy balance[1]

$$\frac{\partial}{\partial t}\int_V \rho e \, \mathrm{d}V + \int_S [\rho e(\boldsymbol{v} - \boldsymbol{v}_s) - \boldsymbol{q}]\cdot \mathrm{d}\boldsymbol{s} = \int_V (\boldsymbol{T} : \operatorname{grad} \boldsymbol{v} + h)\, \mathrm{d}V , \tag{2}$$

- equation of momentum balance or Cauchy's first law of motion

$$\frac{\partial}{\partial t}\int_V \rho \boldsymbol{v} \, \mathrm{d}V + \int_S [\rho \boldsymbol{v} \otimes (\boldsymbol{v} - \boldsymbol{v}_s) - \boldsymbol{T}]\cdot \mathrm{d}\boldsymbol{s} = \int_V \boldsymbol{f} \, \mathrm{d}V , \tag{3}$$

which are valid for an arbitrary part of the continuum of the volume V bounded by the surface S, with surface vector $\mathrm{d}\boldsymbol{s}$ pointing outwards. Here, ρ is the density, $\boldsymbol{v}$ is the continuum velocity vector, $\boldsymbol{v}_s$ is the velocity of the surface S, e is the specific internal energy, $\boldsymbol{q}$ is the heat flux vector, h is the internal energy heat source, $\boldsymbol{T}$ is the stress tensor and $\boldsymbol{f}$ is the resultant body force.

If the problem to be solved involves volumes with moving boundaries ($\boldsymbol{v}_s \neq 0$), then, in addition to the above equations, the so-called

- space conservation law (SCL)

$$\frac{\partial}{\partial t}\int_V \mathrm{d}V - \int_S \boldsymbol{v}_s \cdot \mathrm{d}\boldsymbol{s} = 0 , \tag{4}$$

which links the rate of change of volume V and surface velocity $\boldsymbol{v}_s$, has to be satisfied [4].

It has been assumed here that angular (moment of) momentum balance equation (Cauchy's second law of motion) is satisfied identically, which is true in the great majority of usual engineering

[1] In certain cases it may be preferable, from the numerical stability and accuracy point of view to express energy conservation law in terms of static or total enthalpy, instead of thermal energy (see e.g. [3]).

applications (so-called classical case, when internal angular momenta and internal volume and surface couples are absent).

2.2. Constitutive relations

In order to close the system of Eqs. (1)–(3), information about the response of particular materials to the applied forces is necessary. In this paper the constitutive relations for the thermo-elastic solid and Newtonian fluid are chosen as examples of solid and fluid materials:

- Equations of state

$$\rho = \rho(p, T) \qquad (5)$$
$$e = e(p, T)$$

where p is the pressure and T is the temperature. Common examples are, e.g. $\rho = \text{const}$, $e = c_v T$ valid for incompressible fluids and solids, or $\rho = p/RT$, $e = c_v T$ valid for an ideal gas. Here c_v is the specific heat at constant volume and R is the gas constant.

- Relation between the heat flux and temperature gradient (Fourier's law)

$$q = k \operatorname{grad} T = \frac{k}{\partial e/\partial T} \operatorname{grad} e - \frac{k}{\partial e/\partial T}\frac{\partial e}{\partial p} \operatorname{grad} p \qquad (6)$$

where k is the thermal conductivity.

- Relation between stresses and strains (deformations) in solids (Duhamel–Neumann form of Hook's law)

$$\boldsymbol{T} = 2\eta \boldsymbol{D} + \lambda \operatorname{div} \boldsymbol{w} \boldsymbol{I} - (3\lambda + 2\eta)\alpha(T - T_r)\boldsymbol{I}\,, \qquad (7)$$

where

$$\boldsymbol{D} = \frac{1}{2}[\operatorname{grad} \boldsymbol{w} + (\operatorname{grad} \boldsymbol{w})^{\mathrm{T}}] \qquad (8)$$

is the deformation (strain) tensor, $\boldsymbol{w}$ is the displacement vector, T_r is the reference temperature (which corresponds to a thermally undeformed state), η and λ are Lame's coefficients and α is the linear thermal expansion coefficient.

- Relation between stresses and rate of deformation for fluids (Stokes' law)

$$\boldsymbol{T} = 2\mu \dot{\boldsymbol{D}} - \frac{2}{3}\mu \operatorname{div} \boldsymbol{v} \boldsymbol{I} - p\boldsymbol{I}\,, \qquad (9)$$

where

$$\dot{\boldsymbol{D}} = \frac{1}{2}[\operatorname{grad} \boldsymbol{v} + (\operatorname{grad} \boldsymbol{v})^{\mathrm{T}}] \qquad (10)$$

is the rate of deformation tensor.

2.3. Mathematical model

By introducing constitutive relations into equations governing mass, energy and momentum balance a closed set of 4 equations with 4 unknown functions (e, p, $\boldsymbol{v}$ and $\boldsymbol{w}$) of spatial coordinates and time is obtained. It is important to note that momentum and energy equations can be written in the form of the following generic transport equation

$$\frac{\partial}{\partial t}\int_V \rho B_\phi \,\mathrm{d}V + \int_S [\rho\phi(\boldsymbol{v}-\boldsymbol{v}_s) - \Gamma_\phi \,\mathrm{grad}\,\phi]\cdot \mathrm{d}\boldsymbol{s} = \int_V Q_{\phi V}\,\mathrm{d}V + \int_S Q_{\phi S}\cdot \mathrm{d}\boldsymbol{s}\,, \tag{11}$$

which can be regarded as an equation for ϕ, where ϕ stands for thermal energy, displacement vector in solids, or velocity vector in fluids, or any other transported property (like kinetic energy of turbulence and its dissipation rate, chemical species concentration, etc.), while the continuity equation is usually combined with momentum equation to obtain the pressure. Coefficients B_ϕ and Γ_ϕ are given in Table 1, together with source term $Q_{\phi V}$, which contains actual source term, and $Q_{\phi S}$, which consists of terms coming from the heat flux vector or from the stress tensor which are not contained in $\Gamma_\phi \,\mathrm{grad}\,\phi$.

At this place it may be useful to note the following.

- For a large number of practically relevant fluids and solids the thermal energy can be considered to be function of temperature only, in which case $\partial e/\partial p = 0$, i.e. $Q_{eS} = 0$.
- *In the case of thermo-elastic solid* the continuity equation needs not be considered (it serves for determining density, which is constant). In most of the usual engineering applications it can be assumed that not only deformations (strains), but also the displacements, velocities and accelerations themselves are small, thus the (non-linear) convection terms $\rho e(\boldsymbol{v}-\boldsymbol{v}_s)$ and $\rho\boldsymbol{v}\otimes(\boldsymbol{v}-\boldsymbol{v}_s)$, as well as the mechanical energy dissipation term $\boldsymbol{T}:\mathrm{grad}\,\boldsymbol{v}$ can be neglected and

$$\frac{\partial \boldsymbol{v}}{\partial t} \text{ reduces to } \frac{\partial^2 \boldsymbol{w}}{\partial t^2}\,. \tag{12}$$

Consequently, in solids one has to solve two non-linear equations (energy and momentum balance) with two unknowns (thermal energy e and displacement vector $\boldsymbol{w}$). However, if physical properties of solid can be considered constant, these equations are linear.

- *In fluids*, however, none of the above assumptions hold and the mathematical model consists of three always non-linear equations (continuity, energy and momentum balance) with three unknowns (thermal energy e, velocity vector $\boldsymbol{v}$ and pressure p).
- *In the case of conjugate fluid flow, heat transfer and stress analysis*, solid and fluid regions are in general coupled via energy equation. However, in most practical applications the heat energy source in solids coming from the thermo-elastic dissipation $(3\lambda + 2\eta)\alpha T_r\,\partial(\mathrm{div}\,\boldsymbol{w})/\partial t$, as well as the change of the shape of solid due to deformation can be neglected. In that case calculation of temperature, velocity and pressure field is decoupled from the displacement calculations. However, in order to calculate displacements and resulting stresses in solid, temperature in solids and velocity and pressure fields in fluids have to be known. It will be shown later, however, that the present method does not take and, indeed, does not need to take advantage of these special cases and solves all the equations simultaneously.

To complete the mathematical model, initial and boundary conditions have to be specified. At the *initial* instant of time $t = t_0$ values of all dependent variables have to be known at all points of the solution domain Ω

$$\phi(\boldsymbol{r}, t_0) = \phi^0(\boldsymbol{r})\,, \quad \boldsymbol{r}\in\Omega\,. \tag{13}$$

Table 1
The meaning of B_ϕ and Γ_ϕ and source terms $Q_{\phi V}$ and $Q_{\phi S}$ in Eq. (11)

ϕ	B_ϕ	Γ_ϕ	$Q_{\phi V}$	$Q_{\phi S}$
e	e	$\dfrac{k}{\partial e/\partial T}$	$\boldsymbol{T}:\mathrm{grad}\,\boldsymbol{v} + h$	$-\dfrac{k}{\partial e/\partial T}\dfrac{\partial e}{\partial p}\,\mathrm{grad}\,p$
$\boldsymbol{w}$	$\dfrac{\partial \boldsymbol{w}}{\partial t}$	η	f	$\eta(\mathrm{grad}\,\boldsymbol{w})^{\mathrm{T}} + [\lambda\,\mathrm{div}\,\boldsymbol{w} - (3\lambda+2\eta)\alpha(T-T_r)]\boldsymbol{I}$
$\boldsymbol{v}$	$\boldsymbol{v}$	μ	f	$\mu(\mathrm{grad}\,\boldsymbol{v})^{\mathrm{T}} - \left[\dfrac{2}{3}\mu\,\mathrm{div}\,\boldsymbol{v} + p\right]\boldsymbol{I}$

Due to the elliptic nature of the governing equations *boundary conditions* have to be specified at all times at all solution domain boundaries $\partial\Omega$. A range of boundary conditions is applicable, but they can all be classified into two groups:

- Dirichlet boundary conditions where value of dependent variable at the boundary is given (e.g. prescribed displacements in solids or inlet boundary in fluids)

$$\phi(\boldsymbol{r}_B, t) = f_1(t) , \quad \boldsymbol{r}_B \in \partial\Omega , \tag{14}$$

- Neumann boundary conditions where value of dependent variable gradient at the boundary is specified (e.g. prescribed traction in solids or given heat flux)

$$\text{grad}\, \phi(\boldsymbol{r}_B, t) = f_2(t) , \quad \boldsymbol{r}_B \in \partial\Omega . \tag{15}$$

3. Numerical method

Before Eq. (11) is integrated, several important decisions have to be made concerning: (a) choice of vector and tensor components, (b) space and time discretisation procedure and (c) variable arrangement. An appropriate decision about those options is decisive for the stability, conservativeness and efficiency of a numerical method [5]. In this paper the following choices are made.

(a) Although the complete analysis is carried out in a coordinate-free (invariant) form, which enables any vector and tensor components to be used, vector and tensor components related to a global Cartesian coordinate system are preferred because they lead to a strong conservation form of momentum equations, without terms requiring a smooth numerical mesh.

(b) The space is discretised by an arbitrary unstructured mesh, because it is by now generally accepted that only unstructured meshes are capable of describing accurately complicated 3D geometries. As far as time discretisation is concerned, a fully implicit time differencing is employed, because it allows any time step size to be used without generating unphysical results.

(c) All dependent variables are stored at the cell centre, i.e. a collocated variable arrangement is used. This requires only one set of control volumes to be generated, as opposed to four sets in the case of staggered arrangement.

Details about the implementation of the above options into the present method are given in the next section. After that an iterative solution procedure used to solve a coupled set of non-linear algebraic equations resulting from the integration of governing equations is outlined.

3.1. Discretisation procedure

In order to obtain discrete counterparts of Eq. (11), the solution domain is discretised into a finite number of contiguous control volumes (CV) or cells and time is subdivided into an arbitrary number of time steps. The computational points (nodes) are placed at the centre of each CV, while boundary nodes, needed for the specification of boundary conditions, reside at the centre of boundary cell-faces. The control volume is defined by the coordinates of its vertices and can be of an arbitrary polyhedral shape, i.e. it can have an arbitrary number of cell-faces S_j ($j = 4, 5, 6, \ldots$) (Fig. 1). In the same problem control volumes of different topologies can be used.

After that, Eq. (11) for each control volume is written as follows

$$\underbrace{\frac{\partial}{\partial t}\int_V \rho B_\phi \, \mathrm{d}V}_{\text{Rate of change}} + \underbrace{\sum_{j=1}^{n} \int_{S_j} [\rho\phi(\boldsymbol{v} - \boldsymbol{v}_s) - \Gamma_\phi \, \text{grad}\, \phi] \cdot \mathrm{d}\boldsymbol{s}}_{\text{Convection}} = \underbrace{\int_V Q_{\phi V} \, \mathrm{d}V}_{\text{Diffusion}} + \underbrace{\int_S Q_{\phi S} \cdot \mathrm{d}\boldsymbol{s}}_{\text{Source}} , \tag{16}$$

where n is number of cells which share cell-faces with cell P_0 (so-called nearest neighbours) and ϕ and B_ϕ in the case of momentum equations are now related to the Cartesian displacement w_i ($i = 1, 2, 3$) or velocity v_i ($i = 1, 2, 3$) components.

Eq. (16) has four distinct parts: transient rate of change, convection, diffusion and source. This

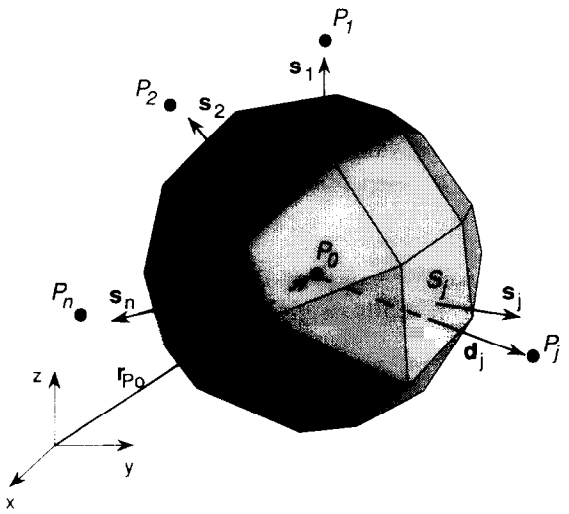

Fig. 1. Control volume of an arbitrary polyhedral shape.

equation is exact, i.e. no approximation has been introduced so far. However, in order to evaluate integrals in the above equation, a distribution of dependent variable ϕ and physical properties of fluid or solid in space and time have to be assumed, and some means of determining surface velocities $\boldsymbol{v}_s$ have to be available.

Spatial distribution

Here, the following linear spatial distribution is employed (although, in principal, any other distribution can be used)

$$\psi(\boldsymbol{r}, t) = \psi_{P_0}(t) + \boldsymbol{g}(t) \cdot (\boldsymbol{r} - \boldsymbol{r}_{P_0}) , \tag{17}$$

when ψ stands for dependent variable ϕ, physical properties of continuum or gradient of ϕ, $\boldsymbol{r}_{P_0}$ is the position vector of point P_0 and $\boldsymbol{g}(t)$ is an approximation of gradient of ψ at point P_0.

The unknown vector $\boldsymbol{g}$ is calculated by ensuring a fit to a set of sampling points usually consisting of nearest neighbours of point P_0, i.e. by solving the following set of equations

$$\boldsymbol{d}_j \cdot \boldsymbol{g} = \psi_{P_j} - \psi_{P_0} \quad (j = 1, \ldots, n) , \tag{18}$$

where $\boldsymbol{d}_j = \boldsymbol{r}_{P_j} - \boldsymbol{r}_{P_0}$ is the distance vector joining point P_0 with its neighbour P_j (Fig. 1). To solve this over determined set of equations the least square method is used, resulting in the following normal equation

$$\mathrm{D}\boldsymbol{g} = \boldsymbol{f} , \quad \text{i.e. } \boldsymbol{g} = \mathrm{D}^{-1}\boldsymbol{f} , \tag{19}$$

where

$$\mathrm{D} = \sum_{j=1}^{n} \boldsymbol{d}_j^{\mathrm{T}} \boldsymbol{d}_j \quad \text{and} \quad \boldsymbol{f} = \sum_{j=1}^{n} \boldsymbol{d}_j^{\mathrm{T}} (\psi_{P_j} - \psi_{P_0}) . \tag{20}$$

It is important to notice that for all ψ's and for assumed linear distribution D is a symmetric 3×3 matrix, whose coefficients depend solely on the mesh geometrical properties and hence, for a given mesh, a single evaluation of D^{-1} suffices.

Formula (17) is used to calculate values of ψ at the cell faces j necessary for evaluation of the surface integrals in (16), leading to a second-order symmetric formula

$$\psi_j^{\mathrm{SO}} = \frac{1}{2}(\psi_{P_0} + \psi_{P_j}) + \frac{1}{2}[(\operatorname{grad}\psi)_{P_0} \cdot (\boldsymbol{r}_j - \boldsymbol{r}_{P_0}) + (\operatorname{grad}\psi)_{P_j}(\boldsymbol{r}_j - \boldsymbol{r}_{Pj})] , \tag{21}$$

where $\boldsymbol{r}_j$ is the position vector of the cell-face centre (Fig. 1). However, for stability reason (in case of

$\psi = \phi$) this value is sometimes blended with some (usually small) amount of a first-order asymmetric (upwind) differencing scheme, which assumes that the value of ϕ at the cell face is calculated as

$$\phi_j^{\mathrm{FO}} = \begin{cases} \phi_{P_0}; & \text{if flow is from } P_0 \text{ to } P_j \\ \phi_{P_j} & \text{if flow is from } P_j \text{ to } P_0 \end{cases} \tag{22}$$

Temporal distribution

As far as temporal distribution of ψ is concerned, according to adopted fully implicit time discretisation of all values of dependent variables are expressed as

$$\psi(\boldsymbol{r}, t) = \psi(\boldsymbol{r}, t_m) = \psi^m , \tag{23}$$

where m is the time step counter and t_m is the current instant of time, except in the transient term where a linear variation of ψ in time is assumed. Henceforth, the time step counter will normally be omitted, and all values of ψ will refer to the current time t_m, unless indicated otherwise.

The main property of the fully implicit differencing is that it does not suffer from the stability related time step restrictions inherent in the otherwise attractive explicit methods [6]. In principle, the magnitude of the time step is limited only by the desired temporal accuracy.

Surface velocity

It is assumed here that the law that governs the motion of the solution domain boundaries, which in turn requires internal CV surfaces to be moved, is known either as a function of time only (e.g. in a piston/cylinder assembly) or as a function of the previous fluid flow development (e.g. free surface flows) or solid body deformation (e.g. metal forming processes: extrusion, drawing, forging, etc.). However, instead of using the SCL to calculate the surface velocities $\boldsymbol{v}_s$ explicitly, we have used equation (4) to calculate the volume flux through the CV faces which results from its motion

$$\sum_{j=1}^{n} \int_{S_j} \boldsymbol{v}_s \cdot \mathrm{d}\boldsymbol{s} = \frac{V_{P_0} - V_{P_0}^{m-1}}{\delta t_m} = \sum_{j=1}^{n} \frac{\delta V_j}{\delta t_m} , \tag{24}$$

where V_{P_0} and $V_{P_0}^{m-1}$ are the volumes of the cell P_0 at times t_m and t_{m-1}, respectively, and δV_j is the volume swept by the cell face S_j during the time interval $\delta t_m = t_m - t_{m-1}$. The swept volume δV_j can easily be calculated when the coordinates of the CV vertices are known at all times, as assumed here.

By using the described spatial and temporal distribution [Eqs. (21)–(23)] and the SCL (24) the evaluation of each term of Eq. (16) will now be described.

Rate of change

Transient term in Eq. (16) is approximated as

$$\frac{\partial}{\partial t} \int_V \rho B_\phi \, \mathrm{d}V \approx \frac{1}{\delta t_m} [(\rho B_\phi V)_{P_0} - (\rho B_\phi V)_{P_0}^{m-1}] , \tag{25}$$

where the meaning of B_ϕ^m and B_ϕ^{m-1} for different ϕ is given in Table 2.

Table 2
Meaning of B_ϕ^m and B_ϕ^{m-1} in Eq. (25) and E_ϕ^m in Eqs. (34)

ϕ	B_ϕ^m	B_ϕ^{m-1}	E_ϕ^m
e	e^m	e^{m-1}	1
w_i	$\frac{1}{\delta t_m} w_i^m$	$\left(\frac{1}{\delta t_m} + \frac{1}{\delta t_{m-1}}\right) w_i^{m-1} - \frac{1}{\delta t_{m-1}} w_i^{m-2}$	$\frac{1}{\delta t_m}$
v_i	v_i^m	v_i^{m-1}	1

Convection flux

The convection flux of the variable ϕ through the CV face j represents the rate at which variable ϕ is convected into (out of) the control volume through cell face S_j and may be approximated as follows

$$C_j = \int_{S_j} \rho\phi(\boldsymbol{v} - \boldsymbol{v}_s)\cdot \mathrm{d}\boldsymbol{s} \approx \dot{m}_j \phi_j^* , \tag{26}$$

where ϕ_j^* stands for the cell-face mean value and $\dot{m}_j$ is the mass flux through cell face j:

$$\dot{m}_j = \int_{S_j} \rho(\boldsymbol{v} - \boldsymbol{v}_s)\cdot \mathrm{d}\boldsymbol{s} \approx \rho_j^* \left(\boldsymbol{v}_j^* \cdot \boldsymbol{s}_j - \frac{\delta V_j}{\delta t_m} \right) . \tag{27}$$

The way cell-face values of density ρ_j^*, velocity $\boldsymbol{v}_j^*$ and convected variable ϕ_j^* are calculated has a strong influence on both accuracy and stability of a numerical method. The velocity $\boldsymbol{v}_j^*$ and density ρ_j^* are obtained from a special interpolation practice which assures a stable solution procedure with collocated grid arrangement as described in the next section, while ϕ_j^* is calculated by blending second-order accurate formula (21) with some small amount of first-order value (22)

$$\phi_j^* = \phi_j^{\mathrm{FO}} + \gamma_\phi (\phi_j^{\mathrm{SO}} - \phi_j^{\mathrm{FO}}) , \tag{28}$$

where γ_ϕ is the blending factor with a value between zero and one, thus combining accuracy of a second-order scheme and stability of a first-order one. It is important to mention that the SO scheme is implemented according to the 'deferred-correction' practice [7], i.e. convective flux is split into implicit part containing the contribution from the FO only and explicit part consisting from the difference between SO and FO contributions.

It should be noticed that for the present choice of constitutive relations the convection term is present in fluids only. However, there are processes of deformation of solids where this term cannot be neglected (plays an important role in the momentum balance), e.g. large deformations of an elastic-viscoplastic solid [8].

Diffusion flux

Diffusion flux D_j of ϕ trough the cell-face j can be approximated by

$$D_j = -\int_{S_j} \Gamma_\phi \,\mathrm{grad}\,\phi \cdot \mathrm{d}\boldsymbol{s} \approx -\Gamma_{\phi j} (\mathrm{grad}\,\phi)_j^* \cdot \boldsymbol{s}_j , \tag{29}$$

where $\Gamma_{\phi j}$ stands for the cell-face mean value of the diffusivity, obtained by using second-order formula (21), and the value of $(\mathrm{grad}\,\phi)_j^*$ is constructed in the following manner

$$(\mathrm{grad}\,\phi)_j^* = (\mathrm{grad}\,\phi)_j + \left[\frac{\phi_{P_j} - \phi_{P_0}}{|\boldsymbol{d}_j|} \frac{\boldsymbol{s}_j}{|\boldsymbol{s}_j|} - \frac{\overline{\mathrm{grad}\,\phi \cdot \boldsymbol{d}_j}}{|\boldsymbol{d}_j|} \frac{\boldsymbol{s}_j}{|\boldsymbol{s}_j|} \right] , \tag{30}$$

where the overbar means an arithmetic average between nodes P_0 and P_j straddling the cell face j and value of $(\mathrm{grad}\,\phi)_j$ is calculated by using second-order formula (21).

The gradient based on expression (21) is second-order space-centred and as such cannot sense the oscillations which have the period twice the characteristic length of the numerical mesh. As a result, once induced unphysical oscillatory profile remains superimposed onto the otherwise smooth spatial variation of the dependent variable. Because of this, a third-order diffusion term (term in [] brackets) is introduced into expression (30) for the cell-face gradient of variable ϕ. This additional diffusion transport smoothes out these unphysical oscillations and, once a converged solution is obtained, it will vanish if the spatial variation of ϕ is linear or quadratic. Otherwise, its magnitude is proportional to the truncation error of the second-order scheme, so it does not affect the second-order behaviour of presented discretisation practice. The problem of decoupling between the adjacent computational points is treated in a similar way by some other authors, not only for the estimation of the diffusion fluxes [9], but also to solve the problem of pressure–velocity decoupling on a collocated grid [10]. This will be shown later.

Contribution to the diffusion flux coming from the second term in Eq. (30) is treated implicitly. The rest of the diffusion flux is due to component of the gradient normal to the distance vector $\boldsymbol{d}_j$ (the 'cross-diffusion') and it vanishes when the grid is orthogonal, and is small compared to the so-called 'normal diffusion' if the grid non-orthogonality is not severe. For this reason it is treated explicitly. This simplifies the coefficient matrix of the resulting set of linear algebraic equations since only the contribution of the nearest neighbours of node P_0 are then treated implicitly.

Source term

The part of the source term coming from the true, volume sources is integrated by assuming a linear variation of the source over the control volume

$$q_{\phi V} = \int_V Q_{\phi V}\, \mathrm{d}V \approx (Q_{\phi V})_{P_0} V_0 \,, \tag{31}$$

while the part coming from the heat flux in energy equation or from the stress tensor in momentum equations is discretised in the same manner as diffusion term

$$q_{\phi S} = \int_S Q_{\phi S} \cdot \mathrm{d}\boldsymbol{s} \approx \begin{cases} \sum_{j=1}^{n} \left(-\dfrac{k}{\partial e/\partial T} \dfrac{\partial e}{\partial p} \operatorname{grad} p \right)_j \cdot \boldsymbol{s}_j & \text{for } \phi = e \\ \sum_{j=1}^{n} \left\{ \left[\mu (\operatorname{grad} \boldsymbol{v})^{\mathrm{T}} - \dfrac{2}{3} \mu \operatorname{div} \boldsymbol{v} \boldsymbol{I} - p \boldsymbol{I} \right]_j \cdot \boldsymbol{i}_i \right\} \cdot \boldsymbol{s}_j \,; & \text{for } \phi = v_i \\ \sum_{j=1}^{n} \{ [\eta (\operatorname{grad} \boldsymbol{w})^{\mathrm{T}} + \lambda \operatorname{div} \boldsymbol{w} \boldsymbol{I} - (3\lambda + 2\eta)\alpha (T - T_{\mathrm{r}}) \boldsymbol{I}]_j \cdot \boldsymbol{i}_i \} \cdot \boldsymbol{s}_j \,; & \text{for } \phi = w_i \end{cases} \tag{32}$$

where $\boldsymbol{i}_i (i = 1, 2, 3)$ are the Cartesian base vectors.

It is often possible to linearise volumetric source term $q_{\phi V}$ and add a part of it to central coefficient of the resulting coefficient matrix which will then increase its diagonal dominance, thus enhancing the convergence of the resulting linear algebraic system. Different practices of linearising source term are suggested by Patankar [11]. It may also be beneficial, from stability and efficiency point of view, to take some parts of the surface source $q_{\phi S}$ into account implicitly, as it was done by Demirdžić and Martinović [12] in the case of momentum equations in solids.

Initial and boundary conditions

To start the calculation, all dependent variables have to be set to their initial values ϕ^0 defined by Eq. (13). However, in the case of the momentum equation in solids, apart from w_i^0, the displacement vector components w_i^{-1} at time $t_{-1} = t_0 - \delta t_0$ are required. If those data are not available, they can be approximated by assuming that $w_i^{-1} = w_i^0$ and $\delta t_0 = \delta t_1$ (which is correct in most practical applications).

The expressions for the evaluation of the convective and diffusive fluxes described above are valid for all interior cell faces. On the faces coinciding with the boundary of the solution domain $\partial\Omega$ boundary conditions (14) or (15) have to be applied. In the case of Dirichlet boundary condition the above formulae remain valid, while in the case of Neuman boundary conditions the boundary fluxes are added to the source term of the adjacent control volume.

Resulting algebraic equations

After assembling all the terms featuring in Eq. (16), it can be written in the form of the following non-linear algebraic equations which links the value of dependent variable ϕ at the control volume centre with its values at the points in the neighbourhood

$$a_{\phi 0} \phi_{P_0} - \sum_{j=1}^{n} a_{\phi j} \phi_{P_j} = b_{\phi} \,, \tag{33}$$

where

$$
\begin{aligned}
a_{\phi j} &= \Gamma_{\phi j}\frac{|\boldsymbol{s}_j|}{|\boldsymbol{d}_j|} - \min(\dot{m}_j, 0)\,,\\
a_{\phi 0} &= \sum_{j=1}^{n} a_{\phi j} + \frac{\rho_{P_0}^{m-1} V_{P_0}^{m-1}}{\delta t_m} E_\phi^m\,,\\
b_\phi &= \sum_{j=1}^{n} \Gamma_{\phi j}\left[(\operatorname{grad}\phi)_j \cdot \boldsymbol{s}_j - \frac{(\operatorname{grad}\phi)_j \cdot \boldsymbol{d}_j}{|\boldsymbol{d}_j|}|\boldsymbol{s}_j|\right]\\
&\quad + \sum_{j=1}^{n} \frac{\gamma_\phi}{2}\dot{m}_j[(\boldsymbol{r}_j - \boldsymbol{r}_{P_0})\cdot(\operatorname{grad}\phi)_{P_0} + (\boldsymbol{r}_j - \boldsymbol{r}_{P_j})\cdot(\operatorname{grad}\phi)_{P_j} + (\phi_{P_j} - \phi_{P_0})\operatorname{sgn}(\dot{m}_j)]\\
&\quad + q_{\phi V} + q_{\phi S} + \frac{\rho_{P_0}^{m-1} V_{P_0}^{m-1}}{\delta t_m} B_\phi^{m-1}\,,
\end{aligned}
\tag{34}
$$

and B_ϕ^{m-1} and E_ϕ^m are defined in Table 2.

3.2. Calculation of pressure

It can be noted that in the above procedure, the pressure featuring in the source term of the fluid momentum equation, has remained unknown, while at the same time no use has been made of the continuity equation. The problem lies in the fact that the pressure does not feature explicitly in the continuity equation which consequently can not be considered as 'an equation for pressure' and the continuity equation comes just as an additional constrain on the velocity field. This constrain can be satisfied only by adjusting pressure field. However, pressure is not a conserved property and has no governing transport equation, so it is not immediately clear how this adjustment of pressure is to be performed. This problem is especially pronounced in case of incompressible fluid flow. At the same time, the pressure source term in momentum equation is calculated using second-order space-centred scheme. As mentioned earlier, such a scheme can produce correct pressure-gradient field, although the underlying pressure field possesses an unphysical oscillatory profile. The simple and yet efficient way of getting around both of these aforementioned problems is to calculate the fluid velocity at a cell face in the following manner

$$
\boldsymbol{v}_j^* = \boldsymbol{v}_j + \delta\boldsymbol{v}_j\,,
\tag{35}
$$

where the first term is the spatially interpolated velocity defined by Eq. (21), while the second term is a third-order pressure diffusion term, defined as

$$
\delta\boldsymbol{v}_j = \left(\frac{\overline{V_{P_0}}}{a_{v0}}\right)\left(\frac{\overline{\operatorname{grad} p}\cdot\boldsymbol{d}_j}{|\boldsymbol{d}_j|} - \frac{p_{P_j} - p_{P_0}}{|\boldsymbol{d}_j|}\right)\cdot\frac{\boldsymbol{s}_j}{|\boldsymbol{s}_j|}\,,
\tag{36}
$$

This term smoothes out oscillatory pressure velocity profile, and at the same time introduces pressure into continuity equation in a manner that a pressure-correction equation can easily be constructed (only the explicit pressure difference across the face in expression (36) is treated implicitly), and the predictor–corrector procedure defined by the SIMPLE algorithm [13] established. The nature and significance of the third-order pressure diffusion term in expression (36) are identical to the one introduced by expression (30) while the diffusion transport of variable ϕ was discussed. Once a converged solution is obtained, this correction term will vanish if the pressure varies linearly or quadratically in space, or it will become small in the limit of a fine grid. In that case the velocity at the cell face will be a simple spatial average, implying that the cell-centre velocities will also satisfy the mass conservation.

Density used in the calculation of the mass flux is calculated as

$$
\rho_j^* = \rho_j^{\mathrm{FO}} + \gamma_\rho(\rho_j^{\mathrm{SO}} - \rho_j^{\mathrm{FO}})\,,
\tag{37}
$$

where blending of the second order accurate SO value with some small amount (typically $\gamma_\rho = 90$ to 95%) of FO value is sometimes necessary for stability reasons.

The so-called *predictor stage* values of $\boldsymbol{v}$, p and ρ (featuring in expressions for $\boldsymbol{v}_j^*$ and ρ_j^*), which satisfy the (linearised) momentum equation, do not necessarily satisfy the continuity equation (1), which can be, by using expression for the rate of change (25) and for the mass flux (27), written in the following form

$$\frac{1}{\delta t_m}(\rho_{P_0} V_{P_0} - \rho_{P_0}^{m-1} V_{P_0}^{m-1}) + \sum_{j=1}^{n} \dot{m}_j = 0 . \tag{38}$$

By employing now the collocated version of the SIMPLE algorithm for compressible flow [14], an equation of the form (33) for pressure correction p' is obtained, with coefficients

$$\begin{aligned} a_{pj} &= \rho_j^* \left(\frac{\overline{V_{P_0}}}{a_{v0}}\right) \frac{|\boldsymbol{s}_j|}{|\boldsymbol{d}_j|} - \left[(1-\gamma_\rho)\min(\boldsymbol{v}_j^* \cdot \boldsymbol{s}_j, 0) + \frac{1}{2}\gamma_\rho \boldsymbol{v}_j^* \cdot \boldsymbol{s}_j\right] \left(\frac{\partial \rho}{\partial p}\right)_{P_j} \beta_p , \\ a_{p0} &= \sum_{j=1}^{n} \hat{a}_{pj} + \frac{V_{P_0}}{\delta t_m} \left(\frac{\partial \rho}{\partial p}\right)_{P_0} , \\ b_p &= -\sum_{j=1}^{n} \dot{m}_j - \frac{1}{\delta t_m}(\rho_{P_0} V_{P_0} - \rho_{P_0}^{m-1} V_{P_0}^{m-1}) , \end{aligned} \tag{39}$$

where all variables have their predictor stage values and a_{v0} is the corresponding momentum equation central coefficient, $\hat{a}_{pj}$ is the 'conjugate' of a_{pj}, i.e. the coefficient related to the cell-face j when P_0 and P_j exchange their roles (when the pressure correction equation for cell P_j is constructed), and $\partial\rho/\partial p$ is calculated from the equation of state (5).

After the field of pressure correction p' is obtained, velocity, pressure and density are *corrected* via

$$\begin{aligned} \boldsymbol{v} &= \boldsymbol{v}_{\text{pred}} + \boldsymbol{v}' = \boldsymbol{v}_{\text{pred}} - \frac{1}{a_{v0}} \sum_{j=1}^{n} p_j' \boldsymbol{s}_j , \\ p &= p_{\text{pred}} + \beta_p p' , \\ \rho &= \rho_{\text{pred}} + \left(\frac{\partial \rho}{\partial p}\right)_{P_0} \beta_p p' , \end{aligned} \tag{40}$$

where β_p is an under-relaxation factor (typically $\beta_p = 0.2$ to 0.3), necessary because the approximations introduced in deriving the pressure-correction equation often result in overestimating the magnitude of p', which in turn leads to slow convergence or divergence of the solution procedure.

Finally, the mass balance satisfying fluxes are calculated as follows

$$\dot{m}_j = \dot{m}_{j,\text{pred}} + \dot{m}' = \dot{m}_{j,\text{pred}} - a_{pj} p_{P_j} + \hat{a}_{pj} p'_{P_0} \tag{41}$$

and used in the consequent calculations of convective fluxes.

It may be worth mentioning that in the case of constant density or low speed (Mach number less than 0.3) variable density flows the density corrections can be neglected, which leads to a pressure correction equation with a symmetric coefficient matrix, which in some situations becomes singular. However, if global mass conservation is enforced properly, the resulting set of linear algebraic equations is undetermined, which practically means that the pressure correction, and consequently the pressure level is undetermined. This, however, has no consequences on the solution, since only pressure gradients, and not the pressure itself, feature in fluid momentum equation.

3.3. Solution procedure

By integrating Eq. (16) over time interval δt_m ($m = 1, 2, \ldots$) and over all N CVs eight mutually coupled sets of N non-linear, algebraic equations with eight unknowns (v_i, w_i, e and p) of the form (33) is obtained. There are a number of possible approaches to the solution of that, by all means impressive,

set of equations. In this paper a segregated approach is employed [15], i.e. these equations are linearised and sets of equations for each dependent variable temporarily decoupled by assuming that coefficients and source terms are known (calculated by using dependent variable values from the previous iteration or the previous time step) resulting in a system of linear algebraic equations of the form

$$\mathrm{A}_\phi \boldsymbol{\phi} = \boldsymbol{b}_\phi \tag{42}$$

for each dependent variable (with pressure correction in place of pressure), where A_ϕ is an $N \times N$ matrix, vector $\boldsymbol{\phi}$ contains values of dependent variable ϕ at N nodal points and $\boldsymbol{b}_\phi$ is the source vector.

The present discretisation practice ensures that matrix A_ϕ has the following desirable properties:

- It is sparse with the number of non-zero elements in each raw equal to the number of nearest neighbours n.
- It is symmetric in the case of pressure correction and displacement vector components.
- It is diagonally dominant [$a_{\phi 0} \geq \sum_{j=1}^{n} a_{\phi j}$, see Eq. (34)], which makes system (42) easily solvable by a number of iterative methods which retain the sparsity of matrix A_ϕ, resulting in very small computer memory requirements. For the present calculations a CG method [16] is used when matrix A_ϕ is symmetric and a CGSTAB method [17] when matrix A_ϕ is asymmetric, both with an incomplete Cholesky preconditioning.

The segregated solution strategy employed enables reuse of the same storage for matrix A_ϕ and vector $\boldsymbol{b}_\phi$ for all dependent variables ϕ, thus requiring only $(n_{\mathrm{av}} + 1)N$ storage locations (n_{av} is an average number of cell faces per CV).

Depending on the way fluid and solid equations are coupled, there is a number of solution strategies, one of which will be outlined here.

Step 1. Provide initial values of dependent variables.
Step 2. Determine the location of CV vertices after time has advanced by δt_m and calculate the swept volumes δV_j. (Only in case of moving mesh).
Step 3. Assemble and solve Eq. (42) for the velocity components in fluids, employing the currently available pressures and mass fluxes.
Step 4. Assemble and solve Eq. (42) for the pressure correction and use calculated values to correct mass fluxes, velocity components and pressure.
Step 5. Assemble and solve Eq. (42) for energy and obtain temperature from the equation of state (5).
Step 6. Update density according to equation of state (5) by using the new values of pressure and temperature (only for compressible fluid), as well as other fluid or solid properties which depend on temperature.
Step 7. Assemble and solve Eq. (42) for the displacement components in solids, using the currently available temperature field and pressure and shear stress forces at the fluid–solid interface.
Step 8. Return to step 3 and repeat until the sum of the absolute residuals for all equations has fallen by a prescribed number (typically three) orders of magnitude.
Step 9. Advance the time by the tim increment δt_m and return to Step 2; repeat until the prescribed number of time steps is completed.

There is no need to solve Eq. (42) to a tight tolerance since coefficients and sources are only approximated (based on the values of dependent variables from the previous iteration/time step) and reduction of the sum of absolute residuals for one order of magnitude normally suffices.

In order to promote stability of this solution method, an under-relaxation is often necessary. This has been introduced in the following (so-called inertial) manner [except for the case of the pressure correction equation, see Eq. (40)], by replacing A_ϕ and $\boldsymbol{b}_\phi$ in Eq. (42) with

$$\mathrm{A}_\phi + \frac{1-\beta_\phi}{\beta_\phi}\mathrm{D}_\phi \quad \text{and} \quad \boldsymbol{b}_\phi + \frac{1-\beta_\phi}{\beta_\phi}\mathrm{D}_\phi \boldsymbol{\phi}^{k-1}, \tag{43}$$

respectively, where β_ϕ is an under-relaxation factor with a value between 0 and 1 (typically 0.8 for fluids

and 0.9 for solids), D_ϕ is a diagonal matrix consisting from the diagonal elements of matrix A_ϕ and $\boldsymbol{\phi}^{k-1}$ is the dependent variable vector from the previous iteration/time step. In addition, this enhances the diagonal dominance of the linearised equations, which improves rate of convergence of most iterative linear equations solvers. Also, if the source term is a function of ϕ_P, a suitable linearisation may provide another positive contribution to the central coefficient.

The number of iterations (Steps 3–8) per time step depends on the size of the time increment δt_m; for smaller δt_m fewer iterations are required to obtain the solution at the time t_m. If only steady state is sought, the temporal accuracy is not important and the solution can be obtained by using a single, infinite time step.

4. Testing and application of the method

The present methodology has been applied in a decoupled manner to solid body stress analysis and to fluid flow predictions, including a prismatic bar stretched by its own weight, a plate with a circular hole subjected to a uniform tension [18], laminar lid driven cavity flow, turbulent flow over a cubic obstacle and swirling turbulent flow inside a gas turbine combustor [19] and the method's stability and accuracy has been assessed by comparing the results of calculations with analytical, numerical and experimental data. In this paper predicted distribution of displacements and stresses in a flat plate with a uniformly distributed heat source are compared with analytical solution. After that, results of calculation of the turbulent flow through a pipe with an orifice plate are compared with experimental data. Finally, an example of coupled solution of fluid flow and stress analysis in an air-cooled internal combustion engine will be presented.

4.1. Plate with a uniform heat source

If a plate of arbitrary planeform and constant thickness $2B$ is subjected to a constant uniform heat source h and set free of surface forces and constant temperature $T = T_0 + T_r$ is maintained at the bottom and top surfaces, while the rest of the plate surface is perfectly insulated, then an analytical solution for temperature and displacement components can be obtained [20]

$$
\begin{aligned}
T - T_r &= T_0 + \frac{h}{2k}(B^2 - z^2), \\
w_x &= \alpha\left(T_0 + \frac{h}{k}\frac{B^2}{3}\right)x, \\
w_y &= \alpha\left(T_0 + \frac{h}{k}\frac{B^2}{3}\right)y, \\
w_z &= \alpha\left(T_0 + \frac{3-\nu}{1-\nu}\frac{h}{k}\frac{B^2}{6}\right)z - \alpha\frac{1+\nu}{1-\nu}\frac{h}{k}\frac{z^3}{6}.
\end{aligned}
\tag{44}
$$

It can also be shown that all stress components are zero, except for

$$
T_{xx} = T_{yy} = \frac{1}{2}\frac{\alpha E}{1-\nu}\frac{h}{k}\left(z^2 - \frac{B^2}{3}\right). \tag{45}
$$

Although the planeform can be of any shape, in order to demonstrate the use of polyhedral cells with different topologies, an initial mesh shown in Fig. 2 is used. The thickness of the plate is set to $2B = 0.12$ m and the plate material is assumed to be elastic with the modulus of elasticity $E = 2 \times 10^{11}$ Pa, the Poisson coefficient $\nu = 0.3$ and the linear thermal expansion coefficient $\alpha = 10^{-5}\,\mathrm{K}^{-1}$. The ratio of the heat source and the thermal conductivity, featuring in expressions (44) and 45), is chosen to be $h/k = 5 \times 10^5\,\mathrm{K\,m^{-2}}$, while the temperature T_0 is set to 0. This gives maximum relative temperature of $T_{max} - T_r = 900$ K at the centre of the plate.

The results of calculations (obtained on the aforementioned initial mesh) in the form of $w_x + w_y$ displacements are given in Fig. 2. However, in order to obtain a more accurate, mesh independent

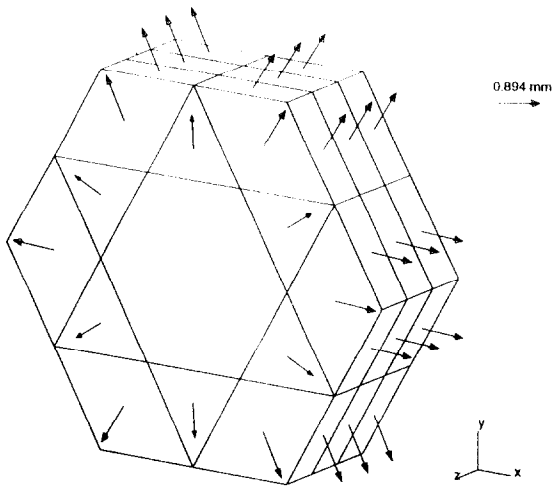

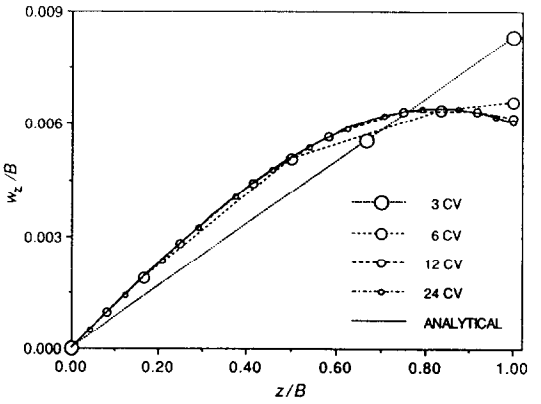

Fig. 2. An initial numerical mesh (39 CVs) and $w_x + w_y$ displacement vectors for the plate with constant uniform heat source.

Fig. 3. Mesh independence test and comparison with analytical solution.

solution, calculations are performed on a number of gradually refined meshes. Since the displacements are linear functions of x and y coordinates, it was sufficient to perform mesh refinement in z direction only. The effects of mesh refinement on the non-linearly varying w_z displacement profile are presented in Fig. 3. The predicted profile converges to the analytical solution as the mesh gets finer, such that the maximum error is less than 1% on a mesh which have 24 CVs in the z direction. The maximum difference between the predicted T_{xx} and T_{yy} stress components and the ones obtained using expression (45) is presented in Fig. 4, showing typical second-order numerical convergence behaviour of the present discretisation practice.

4.2. *Flow through a pipe with an orifice plate*

As the second example, a steady turbulent air flow (Reynolds number 18400) through a circular pipe containing an orifice plate (Fig. 5) is calculated and results are compared with both predictions and 3-D LDA measurements of Nail [21]. To account for the turbulent nature of the flow, the well known $k-\varepsilon$ model of turbulence [22] is employed, requiring the solution of two additional transport equations of the form (16). The temperature and physical properties of the air were treated as constant ($T = 300$ K, $\rho = 1.177\ \mathrm{kg/m^3}$, $\mu = 1.845$ Pa s).

At the upstream solution domain boundary the measured velocity and turbulence quantities are

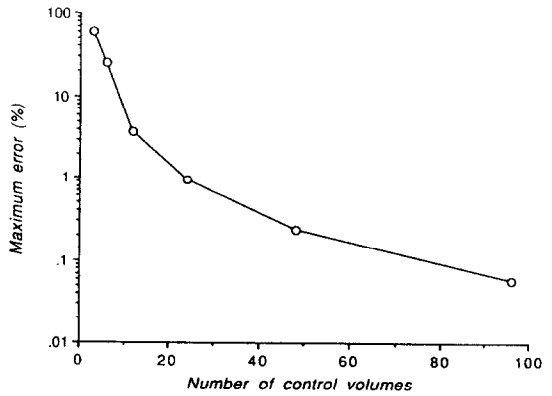

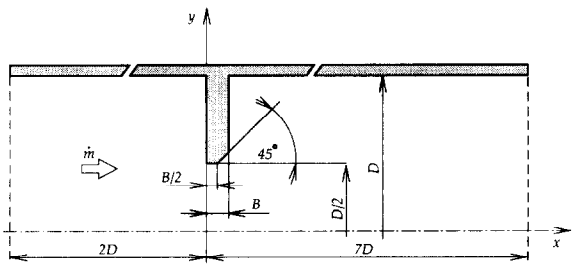

Fig. 4. Maximal error in T_{xx} and T_{yy} versus number of control volumes in z direction.

Fig. 5. Section of the pipe with an orifice plate taken as the solution domain ($D = 25.4$ mm, $B = 3.2$ mm, $\dot{m} = 1.356 \times 10^{-2}$ kg/s).

imposed (Dirichlet boundary conditions), while at the downstream boundary zero gradients of dependent variables are assumed (Neuman boundary conditions). At walls the wall-function approach, devised to account for strong near-wall velocity gradients without requiring a very fine mesh [23], is used.

Since the flow was axi-symmetric, a non-uniform 2D mesh (finer in the regions where high solution variable gradients were detected) consisting of 19308 CVs of different topology (with 4, 5, 6 and 7 cell faces) is used (Fig. 6).

The predicted streamline pattern is shown in Fig. 7 revealing that the reattachment length, an important measure of the quality of numerical results, is well predicted ($x_{r,\mathrm{calc}} = 2.22\ D$, $x_{r,\mathrm{exp}} = 2.25\ D$).

The calculated distribution of the axial velocity vector component v_x along the symmetry axes is compared with predictions and experiments of Nail [21] in Fig. 8. The results obtained are in much closer agreement with experimental data than the predictions of Nail, probably because of the higher

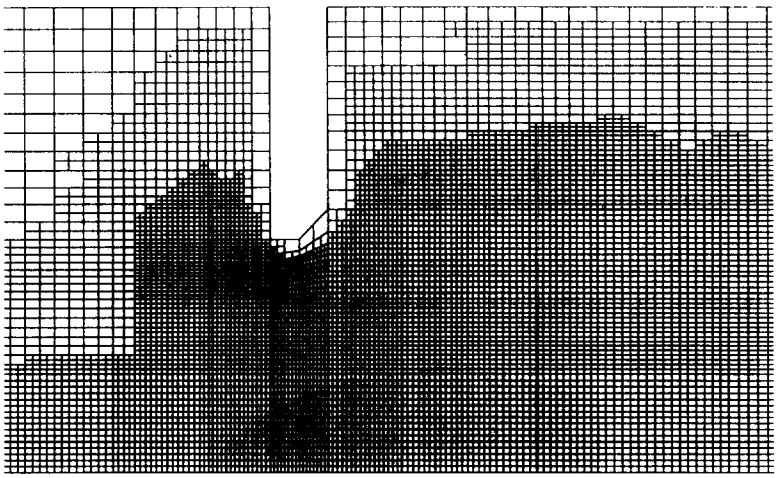

Fig. 6. A detail of the numerical mesh.

Fig. 7. Streamlines.

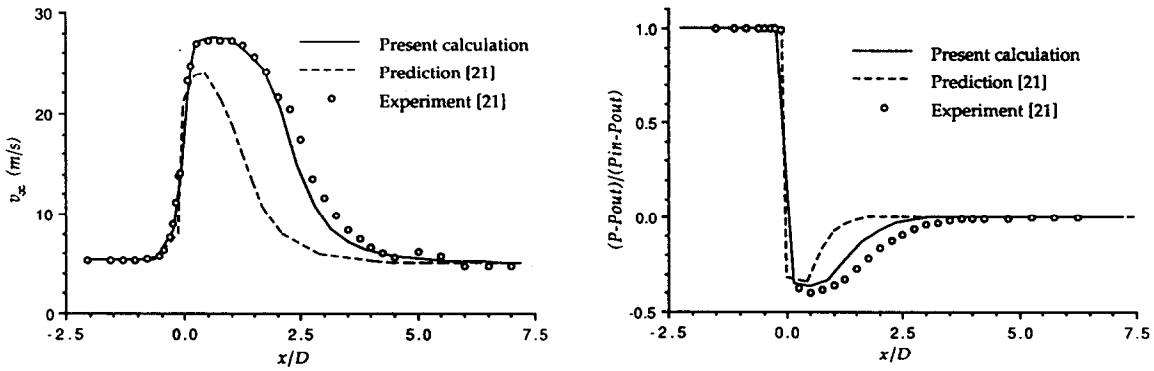

Fig. 8. Axial velocity along the pipe symmetry axes. Comparison with experiments.

Fig. 9. Pipe wall pressure distribution. Comparison with experiments.

mesh resolution and the second-order differencing scheme employed in the present calculations. Although the calculated spreading rate of the jet generated by the orifice plate is a little larger than the measured one, the agreement of the present calculations with experiment can be considered as good.

The variation of wall pressure, presented in Fig. 9, is another significant measure of the quality of the numerical results. Here again, the profiles upstream and downstream of the orifice are in good agreement with the experimental ones. However, immediately after the orifice plate, the calculated wall pressure rises faster than the experiment shows. It is generally accepted that the above discrepancies between calculations and experiments can be attributed to the inadequacy of the $k-\varepsilon$ turbulence model, when applied to the flows with a strong streamline curvature.

4.3. Coupled fluid flow and stress analysis of an air-cooled internal combustion engine

As the final example, a coupled solution of fluid flow in the combustion chamber and stress analysis of the 'engine block' of a one cylinder, air-cooled, two-stroke internal combustion engine (Fig. 10) is presented. Since the objective of this case study is not quantitative comparison with experimental data but only a demonstration of the method's capability, a number of simplifying assumptions are made:

- The intake and exhaust ports (and the associated flow processes) are excluded from the simulations, thus rendering an axi-symmetric solution domain.
- The working fluid is assumed to be an ideal gas with the thermodynamic properties of air. All solid parts are taken to have been made of grey iron.
- The friction force and the blow-by flow between the piston rings-cylinder liner are ignored.
- The piston crown is treated as adiabatic, thus dispensing with the heat transfer and stress analysis in the piston.
- The combustion heat release rate is simulated by a time dependent global heat source function of the engine crank rotation (measured in crank angle from the piston top-dead-centre position).

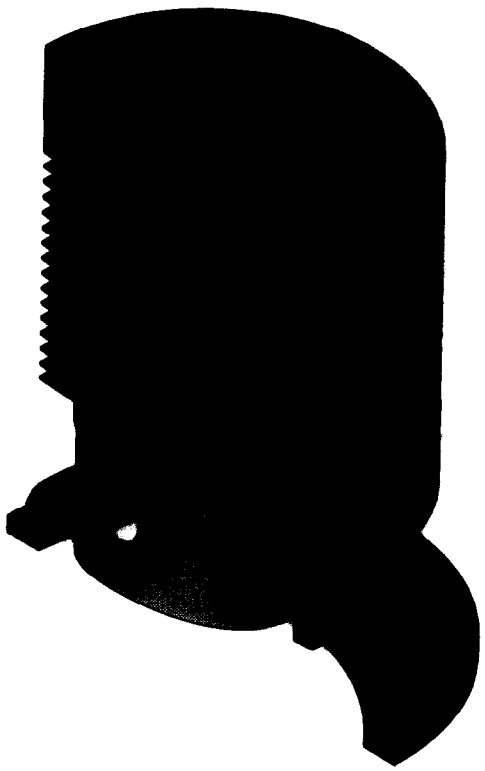

Fig. 10. Simplified one cylinder air-cooled internal combustion engine.

- The heat transfer coefficient between the engine block and the ambient air, as well as the ambient air temperature, is considered constant, thus obviating the need for air flow calculations around the engine block.
- To account for the turbulent nature of the in-cylinder flow, the $k-\varepsilon$ model of turbulence [22] is employed, and to avoid a very fine mesh near the walls, the wall functions [23] are used.

In order to approach a periodic behaviour of dependent variables, the calculations were carried out through several engine cycles till the influence of the (zero) initial conditions became small. In addition, the large heat capacity of the engine block was reduced during the several initial cycles through prescription of a reduced density, thus enabling the engine block to reach its 'operation' temperature in fewer number of cycle simulations.

As far as the boundary conditions are concerned, the no-slip condition in conjunction with wall functions are used for velocities at the solid boundaries. For displacements, zero displacement at the engine block interface to the crank case is assumed; displacement of the rest of the outer engine block is unrestricted. At the liner solid–fluid interface inside the cylinder the fluid pressure, normal and tangential stresses from the fluid side are taken into account. Finally, third-order boundary conditions, i.e. prescribed heat transfer coefficient for the energy equation are applied at all the engine block external surfaces (i.e. solution domain boundaries), except for the piston crown which is considered adiabatic.

Since the accuracy is not a concern, a coarse computational mesh comprising of 1427 CVs in the solid and 3338 CVs in the fluid domains is used for space discretisation. The mesh in the fluid domain moves in concertina fashion according to the piston movement, and is fixed in the solid domain. In Fig. 11 the solution domain and the numerical mesh corresponding to the instant of time when the piston is at the bottom dead centre are shown. The calculations were performed with an integration time step equivalent to 3 degrees of the engine crank rotation angle.

In Fig. 12 velocity fields corresponding to the piston positions at the top dead centre (TDC), at 90 degrees of the crank angle after the TDC (90 DCA ATDC) and at the bottom dead centre (BDC) are shown, illustrating a complex pattern of transient in-cylinder flow structures. The corresponding pressure fields are shown in Fig. 13, depicting a transformation of the pressure field induced by the radial 'squish' flow at TDC to that imposed by the piston motion at BDC. The temporal variations of

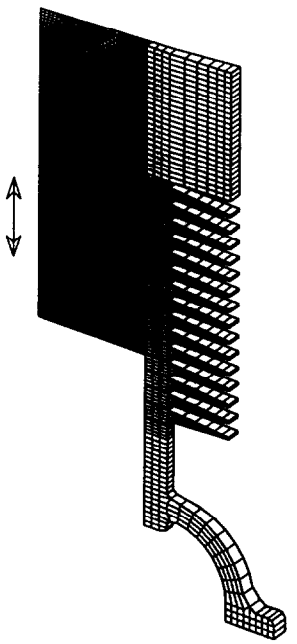

Fig. 11. Solution domain and numerical mesh at the BDC.

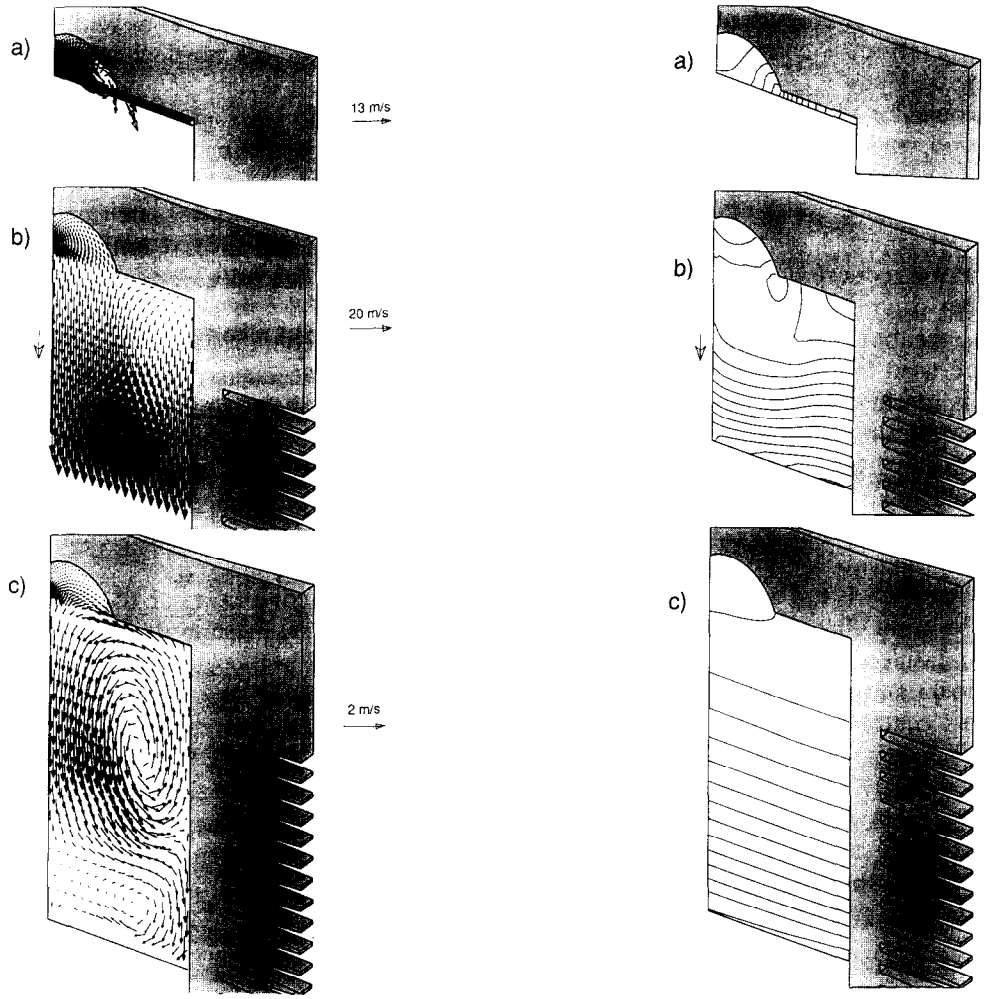

Fig. 12. Velocity fields: (a) at TDC; (b) at 90 CAD ATDC; (c) at BDC.

Fig. 13. Pressure fields: (a) at TDC (contour levels from 10 180 000 to 10 190 400, step 800 Pa); (b) at 90 CAD ATDC (contour levels from 560 500 to 560 630, step 10 Pa); (c) at BDC (contour levels from 210 800 to 211 190, step 30 Pa).

the displacement and stress fields is much less pronounced; thus, they are presented only at 90 DCA ATDC in Fig. 14. Finally, in Fig. 15 the temperature fields in both the fluid and the solid are given at TDC, 90 DCA ATDC and at BDC.

5. Conclusions

The numerical method presented in the paper can be applied to a wide range of problems of continuum mechanics. The examples selected demonstrate its use for problems of deformation of solids and flow of fluids when these phenomena occur separately or together and their simultaneous solution can be beneficial. Although very general as far as its applicability to different geometrical and physical situations is concerned, the method is extremely simple. Namely, a first sight of an arbitrary CV that can be used for the space discretisation (Fig. 1) might suggest that a method which can use such discretisation must involve very complicated mathematics. The fact is, however, that all one has to deal with are vectors and tensors in a global Cartesian coordinate frame (unless someone wishes to do otherwise). As far as the physics is concerned, the method reduces to a straight-forward application of the first principles to a control volume.

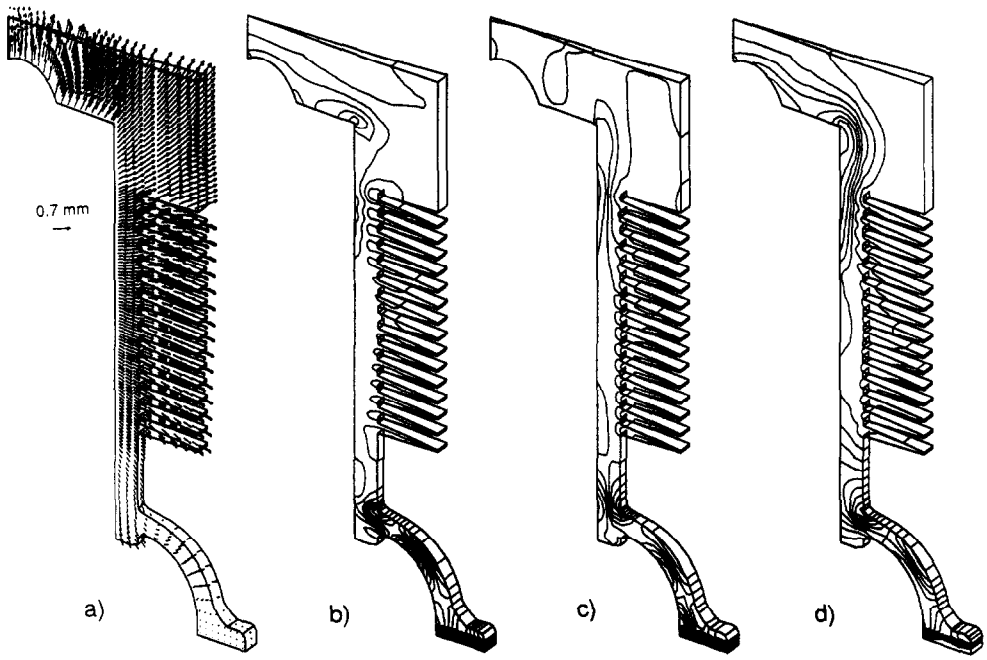

Fig. 14. Displacement and stress fields at 90 CAD ATDC: (a) displacement vectors; (b) T_{xx} (contour levels from −110 to 10, step 10 MPa); (c) T_{yy} (contour levels from −180 to 30, step 15 MPa); (d) T_{zz} (contour levels from −110 to 10, step 10 MPa).

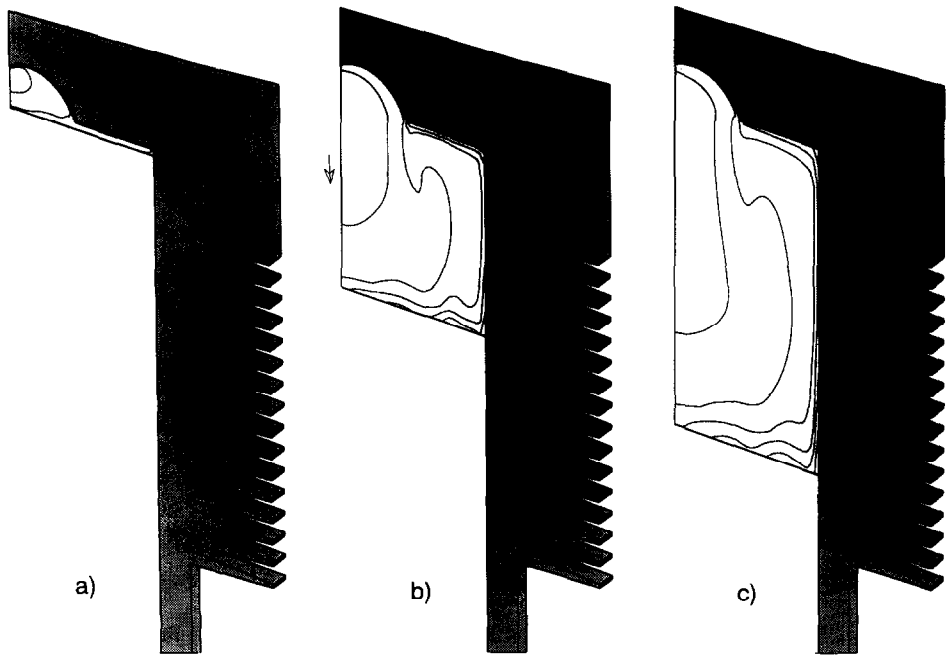

Fig. 15. Temperature fields: (a) at TDC (contour levels from 300 to 1860 step 120 K); (b) at 90 CAD ATDC (contour levels from 300 to 950 step 50 K); (c) at BDC (contour levels from 300 to 820 step 40 K).

The use of moving mesh made of cells of different topologies that can be combined in an arbitrary way is the most general approach to the space discretisation and greatly facilitates the mesh generation for complex geometrical configurations when accurate description of boundaries is desired. This feature is particularly useful for adaptive mesh refinement when injection and depletion of computational points is straightforward and at the same time should help automatic mesh generation, which is rapidly

becoming a very important issue in computational continuum mechanics. The discretisation presented facilitates the use of such meshes. It is performed in real space, using global Cartesian coordinates, thus eliminating the need for coordinate transformation, which makes it easy to understand and implement. The discretisation promotes the conservation of mass, momentum and energy on a discrete level, what, combined with a fully implicit time differencing, enables physically meaningful results to be obtained on very coarse meshes and for large time steps.

The above-mentioned capabilities are built in a computer code, featuring: completely modular structure, allowing new features (e.g. more complicated constitutive relations, additional transport equations) to be built in easily and a very efficient CPU time and memory management characteristic for finite volume programs based on segregated solution algorithms. In addition, the code is fully vectiorisable and, since the computational molecule involves only the nearest neighbours, easily amenable to massive parallelisation.

Further work is being carried out in two main directions. First one is related to improvements in numerical efficiency, which will be effected by implementing an adaptive multigrid technique [19] which greatly reduces the CPU time, especially in the case of linear stress analysis [24], where the absence of the continuity equation (a scalar equation which links all three velocity components in fluids) makes the segregated solution algorithm more sensitive to the inter-equation coupling and by employing a second-order fully implicit time differencing scheme [25], which should considerably increase the time accuracy, albeit on the expense of some additional memory. The second direction deals with the extension of the method's applicability to large deformation analysis of solids (e.g. metal forming processes) and with the accounting for electro-magnetic effects in both fluids and solids (magneto-hydrodynamics, electro-elasticity, etc.). In addition, the code parallelisiation, will enable solutions of very large problems (tens of millions of computational points) to be obtained in a reasonable time using available computer technology.

Acknowledgment

It is the authors' pleasure to thank Dr. B.A. Befrui for his helpful advice regarding the engine simulation.

References

[1] E. Giamei and G.J. Abbascilian, eds., Modelling of Casting and Welding Processes, Vol. 4 (TMS-AIME, Warrendale, PA, USA, 1989).
[2] R.D. Blevins, Flow-Induced Vibration (Van Nostrand Reinhold, New York, 1977).
[3] R.B. Bird, W.E. Stewart and E.N. Lightfoot, Transport Phenomena (Wiley, New York, 1960).
[4] I. Demirdžić and M. Perić, Space conservation law in finite volume calculations of fluid flow, Int. J. Numer. Methods Fluids 8 (1988) 1037–1050.
[5] I. Demirdžić, A finite volume method for computation of fluid flow in complex geometries, Ph.D. Thesis, University of London, 1982.
[6] R.D. Richtmyer and K.W. Morton, Difference Methods for Initial Value Problems, 2nd edition (Wiley-Interscience, London, 1967).
[7] P.K. Khosla and S.G. Rubin, A diagonally dominant second-order accurate scheme, Comput. Fluids 2 (1974) 207–209.
[8] S. Ghosh and N. Kikuchi, An arbitrary Lagrangian–Eulerian finite element method for large deformation analysis of elastic-viscoplastic solids, Comput. Methods Appl. Mech. Engrg. 86 (1991) 127–188.
[9] D.A. Caughy and A. Jameson, Basic advances in the finite volume method for transonic potential flow calculations, in: T. Cebeci, ed., Numerical and Physical Aspects and Aerodynamic Flows (Springer, Berlin, 1982).
[10] C.M. Rhie and W.L. Chow, Numerical study of the turbulent flow past an airfoil with trailing edge separation, AIAA J. 21 (1983) 1525–1532.
[11] S.V. Patankar, Numerical Heat Transfer and Fluid Flow (McGraw-Hill, New York, 1980).
[12] I. Demirdžić and D. Martinović, Finite volume method for thermo-elasto-plastic stress analysis, Comput. Methods Appl. Mech. Engrg. 109 (1993) 331–349.
[13] S.V. Patankar and D.B. Spalding, A calculation procedure for heat, mass and momentum transfer in three-dimensional parabolic flows, Int. J. Heat Mass Transfer 15 (1972) 1787–1806.

[14] I. Demirdžić, Ž. Lilek and M. Perić, A collocated finite volume method for predicting flows at all speeds, Int. J. Numer. Methods Fluids 16 (1993) 1029–1050.
[15] J.P. Van Dormal and G.D. Raithby, An evaluation of the segregated approach for predicting incompressible fluid flows, National Heat Transfer Conference, Denver Colorado (1985).
[16] J.A. Meijerink and H.A. Van Der Vorst, An iterative solution method for linear systems of which the coefficient matrix is a symmetric M-matrix, Math. Comp. 31 (1977) 148–162.
[17] P. Chin, E.F. D'Azevedo, P.A. Forsyth and W.-P. Tang, Preconditioned conjugate gradient methods for the incompressible Navier–Stokes equations, Int. J. Numer. Methods Fluids 15 (1992) 273–295.
[18] I. Demirdžić and S. Muzaferija, Finite volume method for stress analysis in complex domains, Int. J. Numer. Methods Engrg. 37 (1994) 3751–3766.
[19] S. Muzaferija, Adaptive finite volume method for flow predictions using unstructured meshes and multigrid approach, Ph.D. Thesis, University of London, 1994.
[20] A.B. Boley and H.J. Weiner, Theory of Thermal Stresses (Wiley, New York, 1962).
[21] G.H. Nail, A study of 3-dimensional flow through orifice meters, Ph.D. Dissertation, Texas A&M University, 1991.
[22] W.P. Jones and B.E. Launder, The calculation of low-Reynolds-number phenomena with a two-equation model of turbulence, Int. J. Heat and Mass Transfer 15 (1972) 301–314.
[23] B.E. Launder and D.B. Spalding, The numerical computation of turbulent flows, Comput. Methods Apl. Mech. Engrg. 3 (1974) 269–289.
[24] S. Muzaferija and I. Demirdžić, Finite Volume solid body stress analysis using adaptive unstructured meshes and multigrid acceleration technique (to be published).
[25] M. Arnal, O. Lauer, Ž. Lilek and M. Perić, Prediction of three-dimensional unsteady lid-driven cavity flow, in: M. Deville et al., ed., Numerical Simulation of 3-D Incompressible Unsteady Viscous Laminar Flows, Notes on Numerical Fluid Mechanics, Vol. 36 (Vieweg, Braunschweig, 1992).